Confinement and Transport Studies of Conventional Scenarios in ASDEX Upgrade

F. Ryter, J. Stober, A. Stäbler, G. Tardini, H. - U. Fahrbach, O. Gruber, A. Herrmann, F. Imbeaux[1], A. Kallenbach, M. Kaufmann, B. Kurzan, F. Leuterer, M. Maraschek, H. Meister, A. G. Peeters, G. Pereverzev, A. Sips, W. Suttrop, W. Treutterer, H. Zohm and ASDEX Upgrade Team

Max-Planck-Institut für Plasmaphysik,EURATOM-IPP Association, Germany
[1] CEA-Cadarache DRFC,France

e-mail contact of main author: ryter@ipp.mpg.de

Abstract. Confinement studies of conventional scenarios, i.e. L and H modes, in ASDEX Upgrade indicate that the ion and electron temperature profiles are generally limited by a critical value of $\nabla T/T$. When this is the case the profiles are stiff: core temperatures are proportional to pedestal temperatures. Transport simulations based on turbulence driven by Ion Temperature Gradient show good agreement with the ion experimental data. Studies specifically dedicated to electron transport using Electron Cyclotron Heating in steady-state and modulated indicate that electron temperature profiles are also stiff, in agreement with recent calculations on transport driven by ETG turbulence with streamers. In particular the predicted threshold and the increase of the stiffness factor with temperature are found experimentally. The density profiles are not stiff. As a consequence of this profile behaviour, the plasma energy is proportional to pedestal pressure and improves with density peaking. The confinement time increases with triangularity and can be good at densities close to the Greenwald limit. In this operational corner and at $q_{95} \approx 4$, the replacement of type-I ELMs by small ELMs of type-II provides good confinement with much reduced peak power load on the divertor plates.

1. Introduction

Investigations on confinement are carried out in the ASDEX Upgrade divertor tokamak (major radius R = 1.65 m, minor radius a = 0.5 m, elongation $\kappa \approx 1.6$). The present work deals with conventional scenarios, i.e. L and H mode discharges *without* internal barriers. Recently the experimental possibilities of the tokamak have been improved: i) achievement of higher triangularity up to 0.4; ii) upgrade of one of the two NBI lines (10 MW each) from 60 kV to 93 kV; iii) increase of the Electron Cyclotron Heating (ECH) system from 1 to 2 MW /2 s. As reported earlier [1, 2], temperature profiles in ASDEX Upgrade are generally "stiff", limited by a maximum value of $\nabla T/T$. This property is investigated in detail.

2. Physics of temperature profile stiffness

Ion Temperature Gradient (ITG) driven modes are believed to be the main origin of turbulence causing the anomalous transport through the ion channel, [3, 4, 5, 6]. Recent calculations [7] indicate that Electron Temperature Gradient (ETG) turbulence may lead to a large transport because radially extended large cells, so-called streamers, can develop. The properties of temperature gradient (TG) driven turbulence for ions and electrons are qualitatively similar. They lead to a limitation of the temperature profiles by a critical value of $\nabla T/T$. The heat transport can be expressed as:

$$\chi = T^{3/2}[\xi_0 + \xi_{TG} \cdot G(\nabla T/T - (\nabla T/T)_c)] \quad (1)$$

Here χ is the heat diffusivity, ξ_0 represents transport without TG turbulence, $\xi_{TG} \cdot G$ represents the transport by TG turbulence. The function G is equal to zero for $\nabla T/T \leq (\nabla T/T)_c$ but

increases strongly when $\nabla T/T > (\nabla T/T)_c$ and the transport is high and very sensitive to variations in $\nabla T/T$ which keeps the profiles close to $(\nabla T/T)_c$. G eventually saturates [5, 8]. The factor $T^{3/2}$ reflects the gyro-Bohm assumption and causes an increase of stiffness with temperature. These considerations are not necessarily valid inside the sawtooth inversion radius where profiles may be limited by the MHD activity. This profile stiffness is reflected in practice by the fact that the core temperatures are proportional to the temperature in the edge region, or equivalently that the profiles plotted on a logarithmic scale are shifted vertically according to their edge temperature. The edge (or pedestal) temperature is an essential parameter for the profile behaviour.

3. Temperature profile stiffness in NBI-heated H-modes

The profile stiffness could be studied in more detail by comparing discharges heated with 60 kV and 93 kV. At high plasma densities the 60 kV and 93 kV NBI beams result in rather different beam deposition profiles. This was done in type-I ELMy H-modes at $1.0 \times 10^{20} m^{-3}$. The measured temperature profiles are unaffected by the change in beam energy. The heat flux in the core of the plasma is significantly higher for 93 kV compared to 60 kV beams. At $\rho = 0.4$ the difference amounts to almost a factor of 2. As a results, across the whole plasma χ_{eff} for 60 kV is below the value for 93 kV beams, with a difference reaching a factor of 2 despite the very similar temperature profiles. Obviously, the heat conductivity adjusts itself to maintain the observed stiff temperature profiles. This behaviour is independent of triangularity.
In addition to these studies, a database including profile data from about 30 H-mode with NBI, [6], indicates that the ion profiles are quite stiff. Simulations of these discharges using three models based on ITG and Trapped Electron Modes physics for ions and electrons respectively, (IFS/PPPL [3], GLF23 [9], Weiland [10]), agree well with the ion data, see also [11]. The behaviour of the electron profiles is less clear: in the middle and high density range, the electron profiles are stiff, similarly to the ions. However, in the low density range, the core electron temperatures become flatter than expected from the proportionality to the pedestal temperature extrapolated from the behaviour at higher density. This happens at high electron pedestal temperatures as reported earlier for ASDEX Upgrade [2] and also observed for JET [12]. The reason for this behaviour in ASDEX Upgrade is attributed to the fact that, at low density and high temperatures, the heat flux from the NBI into the ion channel is high, but that into the electron channel is low and not sufficient over a large part of the central plasma for the T_e profiles to reach $(\nabla T_e/T_e)_c$.

4 Characterisation of electron temperature profile stiffness using ECH

The stiffness of the electron temperature profiles has been addressed specifically using ECH in steady-state and power modulation experiments. We first concentrate on a set of experiments in which we heated plasmas in the center using either 0.8 MW or 1.6 MW of ECH power. The resulting temperature profiles including the reference with Ohmic heating are plotted on a logarithmic scale in Fig. 1. The profiles have a similar shape and are shifted according to their edge temperature. The shadowed area indicates a region where the slope of the profiles, i.e. $\nabla T_e/T_e$, is the same. In the center ($r < 0.25$m) the slope changes and is different for each profile. The knee of each profile at $r \approx 0.25$ m caused by the slope change is clearly outside the inversion radius of the sawteeth ($r_{inv} \approx 0.22$ m). We identify the radial position of the knee as the point from which outwards the electron heat flux is high enough for T_e to reach $(\nabla T_e/T_e)_c$. Towards the edge the profiles gradually deviate from the constant slope which seems to occur for T_e below ≈ 600 eV.

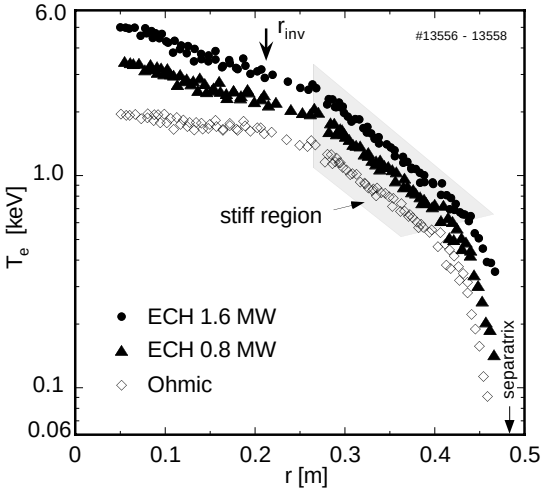

Figure 1: *T_e profile for central ECH heating at 0.8 MW and 1.6 MW, and from the preceding Ohmic phase. r in LFS equatorial plane.*

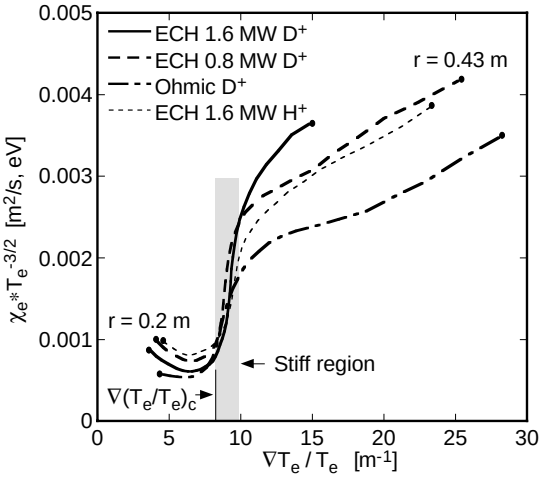

Figure 2: *χ^{PB} normalized by gyro-Bohm assumption $T_e^{3/2}$ versus $\nabla T/T$ for discharges without ECH and with 0.8 MW and 1.6 MW.*

Power scans of ECH in discharges at three different plasma current (I_p = 0.6, 0.8, 1.0 MA, B_T = 2.3 T) exhibit similar properties. In particular, in the stiff region the value of $\nabla T_e/T_e$ does not depend on I_p. Obviously in these L-modes $(\nabla T_e/T_e)_c$ does not depend on plasma current which implies, that the well-known improvement of confinement (and temperature) with I_p is provided by an increase of the edge temperature with I_p.

Following Eq. 1 we plot in Fig. 2 $\chi_e/T_e^{3/2}$ versus $\nabla T_e/T_e$ for the discharges of Fig. 1. The result from a similar discharge in hydrogen indicates that the electron transport is not sensitive to the ion mass. The curves exhibit the expected properties: they coincide for $\nabla T_e/T_e \leq (\nabla T_e/T_e)_c$, have the same threshold $(\nabla T_e/T_e)_c$ as well as the same increase above the threshold and they saturate for large values of $\nabla T/T$. The value of the threshold does not depend on temperature or heat flux as shown by the overlap of the three curves in this region. The normalisation by $T_e^{3/2}$ works well, suggesting that the gyro-Bohm assumption is correct. These curves are not plotted at constant temperature, as one would do following Eq. 1. Therefore, their levelling off is not attributed to the saturation of the turbulence intensity at given T_e, but is believed to be due to the decrease of stiffness at low temperatures, below $\approx$ 600 eV. This latter property is also in qualitative agreement with ETG calculations which indicate that the appearance of streamers requires a minimum value of temperature, [8]. Complementary to these experiments with central ECH, discharges with off-axis ECH indicate that transport indeed decreases in the region between plasma axis and ECH deposition, accordingly to the decrease of $\nabla T_e/T_e$ below the critical value, [13].

The steady-state analyses were extended with ECH power modulation experiments which confirm that the change in transport for off-axis ECH cases is caused by a change of diffusivity and cannot be attributed to convection. In each shot we first launched, as reference, heat pulses with one modulated gyrotron (M) depositing at $\rho_t \approx 0.7$, (ρ_t = normalized flux radius). Later in the same discharge we added at mid-radius ($\rho_t \approx 0.5$) a CW ECH pulse ($\approx$ 0.8 MW) with gyrotrons (C). This determines three radial regions indicated in Fig 3 a: "central", "intermediate" and "outer" region. In the central region $\nabla T_e/T_e$ drops below the critical value when (C) are switched on. In the two other regions the T_e profile is driven harder against the critical value and is expected to become stiffer. The propagation of the heat pulses launched by M, without and with heating by (C), is analysed using the standard method based on Fourier transform of

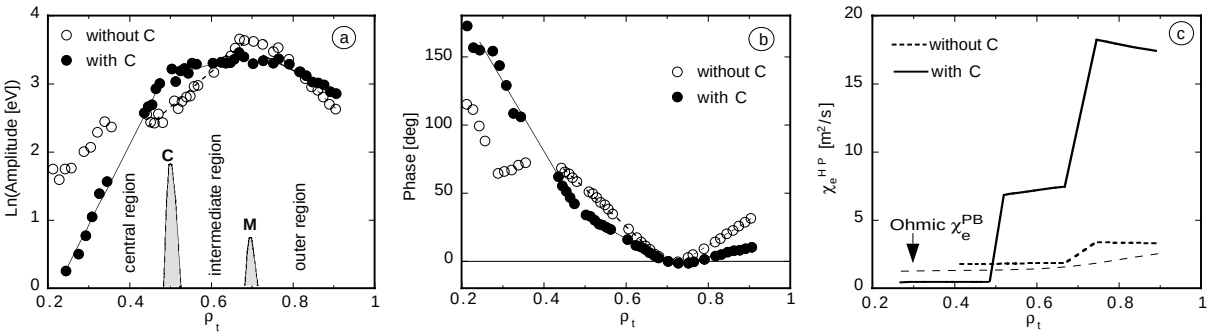

Figure 3: *(a) and (b): Profiles of Fourier data of the heat pulses launched by (M), without and with (C) as indicated in the legend. (c): corresponding χ_e^{HP} profiles.*

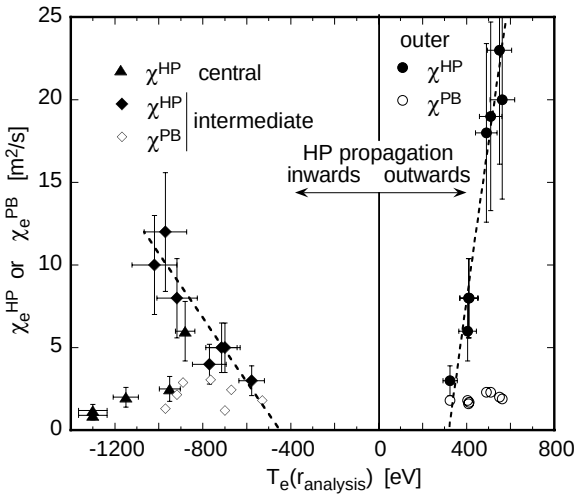

Figure 4: χ_e^{HP} *for outward* ($\rho_t = 0.8$) *and inward* ($\rho = 0.6$) *propagating pulses, as well as the corresponding* χ_e^{PB}. *Negative temperatures means inward propagating pulses.*

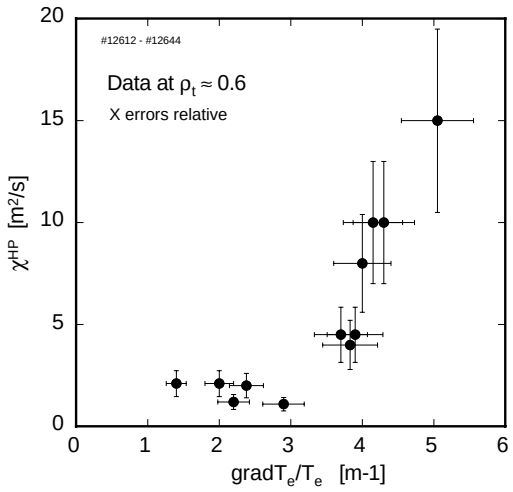

Figure 5: χ_e^{HP} *measured at* $\rho_t = 0.6$ *plotted versus* $\nabla T_e/T_e$. *The variation in* $\nabla T_e/T_e$ *was provided by varying ECH power and deposition around* $\rho_t = 0.6$

the T_e modulation, [14]. The corresponding transport coefficient χ_e^{HP} is deduced from the solution of the linearized diffusion equation in slab geometry, [14], with corrections for cylindrical geometry and effect of density gradient, [15]. The ratio χ_e^{HP}/χ_e^{PB} characterizes the stiffness of the profile. The results of the propagation of the heat waves launched by (M) are shown in Fig 3.

Without (C), the heat pulses propagate smoothly towards the center (Fig 3 a, b) and χ_e^{HP} is low, close to χ_e^{PB}, (Fig 3 c). When gyrotrons (C) are turned on the propagation of the heat pulses in the outer and intermediate regions becomes much faster (flatter gradient of both amplitude and phase), whereas the propagation speed in the central region decreases dramatically (steeper gradient of amplitude and phase), as shown by the corresponding values of χ_e^{HP}.

In the stiff region, the pulses propagating outwards (outer region) and inwards (intermediate region) yield different values of χ_e^{HP}. This is explained by the fact that the heat pulses tend to locally increase or decrease $\nabla T_e/T_e$ depending on their direction of propagation. Varying the power of (C) from 0.44 MW to 0.98 MW changes T_e and influences the propagation in the three regions. The results are shown in Fig 4 versus T_e at the radius of the analysis of χ_e^{HP}. The ratio χ_e^{HP}/χ_e^{PB} strongly increases with temperature and depends on the direction of the pulses. The lines point to similar off-sets indicating a threshold in T_e. We also verified, by varying the radial position of (C), that the boundary between the region with high and low values of χ_e^{HP} coincides

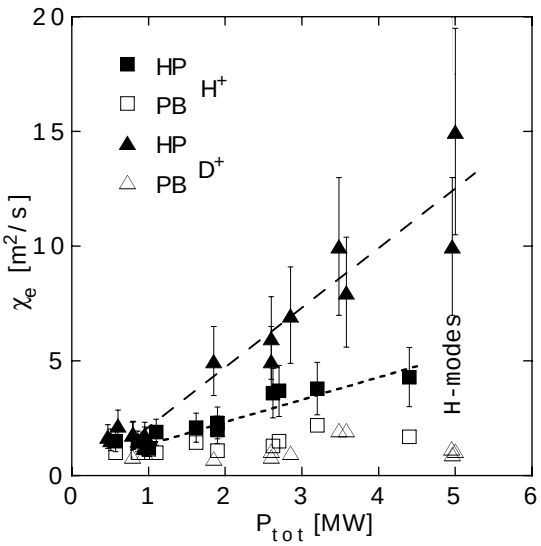

Figure 6: χ_e^{HP} *and* χ_e^{PB} *versus total heating power for hydrogen and deuterium plasmas. Data taken in the region* $0.6 \leq \rho_t \leq 0.8$*, for outwards propagating heat pulses for* χ_e^{HP}*. The deuterium points at* $P_{tot} > 4$ *MW are H-modes, the other points are Ohmic or NBI heated L-modes.*

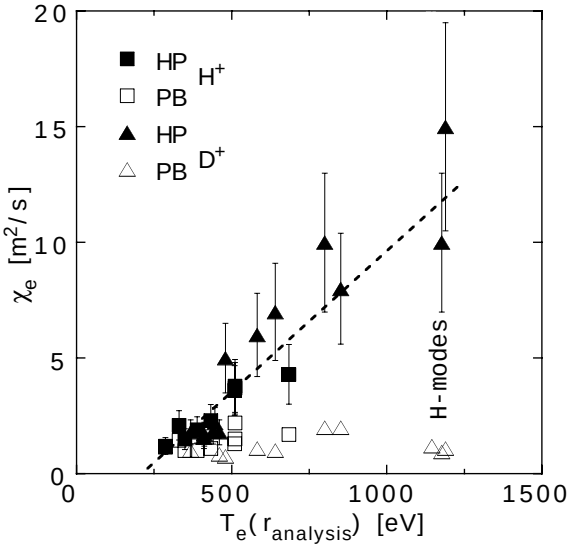

Figure 7: χ_e^{HP} *and* χ_e^{PB} *versus temperature for hydrogen and deuterium plasmas. Data taken in the region* $0.6 \leq \rho_t \leq 0.8$*, for outwards propagating heat pulses for* χ_e^{HP}*. The deuterium points at* $T_e > 1000$ *eV are H-modes, the other points are Ohmic or NBI heated L-modes.*

with the position of (C). Finally, the same experiments in hydrogen yield *quantitatively* the same results: here also the isotope mass does not influence the electron transport.
In a similar type of experiments we again launched heat waves from the edge and analysed their propagation at a given radius (here $\rho_t \approx 0.6$). We varied $\nabla T_e/T_e$ at that radial position by an adequate scan of power and radial location of the absorption layer of other gyrotrons (C). The result is given in Fig. 5. It clearly shows a threshold in $\nabla T_e/T_e$ with a strong increase of χ_e^{HP} by about one order of magnitude for a small variation in $\nabla T_e/T_e$. Whereas the low values of χ_e^{HP} are close to χ_e^{PB} the high ones are larger by at least a factor of 5.
Finally, we applied ECH modulation in Ohmic or NBI heated L and H modes. The total heating power was varied with NBI. The ECH power is at most 20% of the total heating power and the relative temperature perturbation below 10%. In these experiments also, a fast propagation of the outwards propagating pulses is measured. The values of χ_e^{HP} obtained from these pulses increase with total heating power and are much larger than χ_e^{PB} at high power (Fig. 6). For a given heating power, the absolute values of χ_e^{HP} are *lower* in hydrogen than in deuterium, in contradiction with the well-known isotope effect of confinement in which transport deduced from power balance is *higher* in hydrogen than in deuterium. As shown by Fig. 7, a strong positive temperature dependence of χ_e^{HP} is found, similarly to Fig 4. It also exhibits a finite value of T_e as χ_e^{HP} is extrapolated to zero. Moreover, in this plot T_e unifies hydrogen and deuterium for χ_e^{HP}: the apparent contradiction on isotope effect between χ_e^{PB} and χ_e^{HP} is due to the temperature dependence of the stiffness factor.

5. Density profiles

Here we discuss the density behaviour with gas puffing only. In the following we consider the thermal confinement τ_{th} defined as usual. An example is given in Fig 8 for constant gas puffing. Due to the constant external gas flux, the line averaged density increases and exceeds

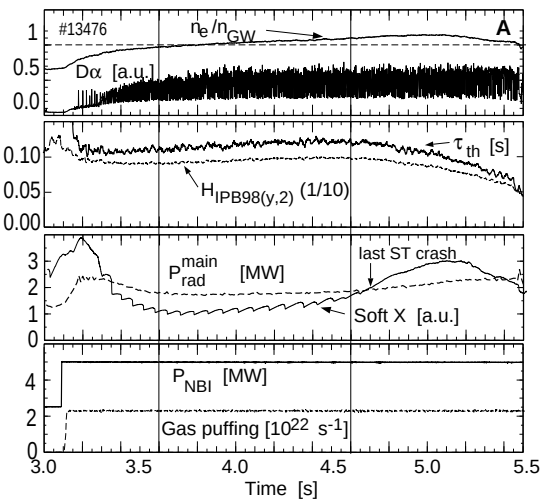

Figure 8: *Time evolution of a discharge with constant gas puffing.*

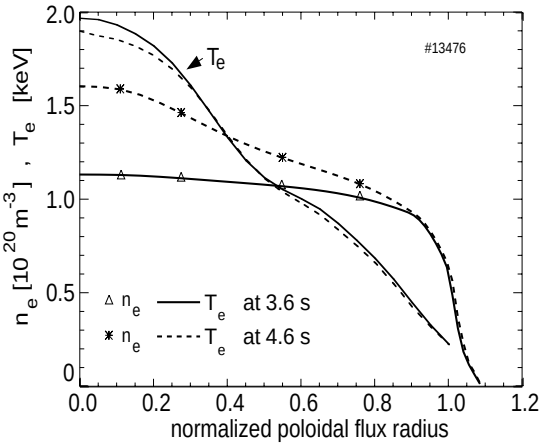

Figure 9: *Electron density and temperature profiles at 3.6 s and 4.6 s of the discharge shown in Fig. 8*

$n_{GW} \approx 10^{20} m^{-3}$ from 4.0 s onwards. After an initial decrease the confinement time increases by 15% until 4.7 s where it decreases due to high central radiative power. This is a consequence of the loss of the sawteeth followed by accumulation of heavy impurities in the center. Before the accumulation Z_{eff} is below 1.3 in the plasma core. With gas puffing the edge density increases first and the profile broadens. On a longer time scale the density profiles peaks significantly, as shown in Fig 9. The pedestal and SOL regions which are determined by the particle source remain unchanged. The density profiles are not stiff in contrast to the temperature profiles which do not change (Fig 9). The flattening of the density profile together with temperature profile stiffness are the reasons for the decrease of confinement observed at the beginning of the gas pulse. The heat flux was changed in the experiment by varying the heating power and its deposition profile combining NBI (slightly hollow heating profile) and ICRH (central heating). It turns out that the particle source by the NBI cannot be the only reason for the density peaking: an inward particle pinch is involved. These experiments indicate a correlation between χ and the particle diffusion coefficient D: the density profiles becomes flat when central heating is increased. These observations are supported by applying ECH in various types of discharges which react to this additional heating with flatter density profiles. In these experiments one may speculate that ECH increases the electron heat flux and thus the ETG turbulence level. This so-called density "pump-out" was observed earlier in other devices with ECH, e.g. in the stellarator W7-AS [16].

6. Global confinement

Due to profile stiffness, for a given shape of the density profile, the plasma energy is expected to be proportional to the pedestal pressure. This is shown in Fig. 10, for ≈ 300 representative discharges grouped in two triangularity ranges: $0.1 \leq \delta < 0.25$ and $0.25 \leq \delta \leq 0.4$.

The figure shows a strong correlation between electron pedestal pressure $p_{e,ped}$ and thermal plasma energy and a positive influence of δ as well. A linear regression yields:

$$W_{th} \propto p_{e,ped}^{0.75} P_{heat}^{0.14} \tag{2}$$

with low RMSE value of about 10%. This representation provides a unification of discharges with different ELM types and run at various values of plasma current and triangularity. Including these variables in the regression indicates that they are not significant. Another regression

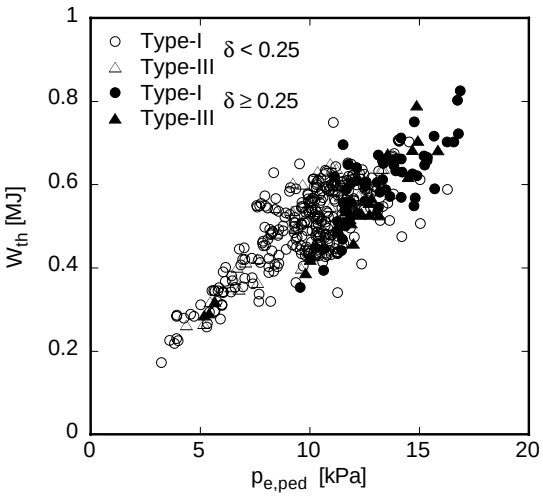

Figure 10: *Thermal plasma energy versus pedestal electron pressure ($\rho_{pol} = 0.8$).*

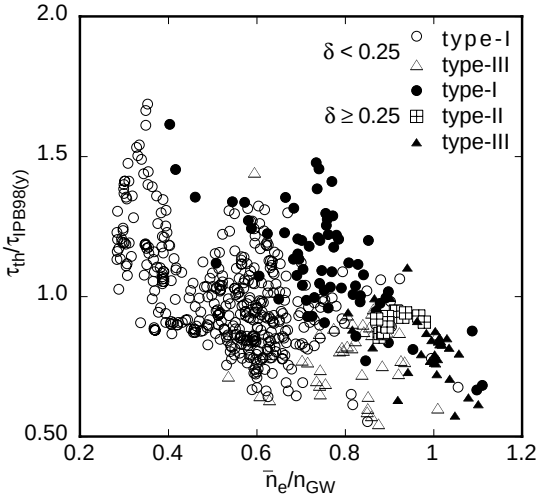

Figure 11: *Thermal confinement normalized by $\tau_{IPB98(y)}$ versus normalized density.*

provides a quantitative dependence of $p_{e,ped}$ upon δ:

$$p_{e,ped} \propto I_p^{1.4} P_{heat}^{0.2} \delta^{0.3} \tag{3}$$

The dependence upon I_p does not quite reach I_p^2 expected from MHD stability, which might be due to changes in the pedestal region of other quantities influencing stability, e.g. magnetic shear. An overview of the confinement data is provided in Fig. 11 for τ_{th} normalised by the IPB98(y) ELMy H-mode τ scaling, [17]. This figure exhibits a large scatter at given value of $\bar{n}_e/n_{GW}$ which corresponds to RMSE $\approx$ 20%, which is due to the effect of δ which is not included in the scaling and to the $\bar{n}_e^{+0.41}$ dependence in IPB98(y) which does not represent the data correctly. This positive dependence in IPB98(y) strongly accentuates the degradation of $\tau_{th}/\tau_{IPB98(y)}$ appearing in Fig. 11. As discussed in Sect. 2.3, the shape of the density profiles varies which is also indicated by the confinement database used here: The density profiles are more peaked at low density than at high density. To take this into account we include as regressors the central density $n_e(0)$ and the density in the scrape-off layer averaged over 6 cm starting from the separatrix outwards $n_{e,SOL}$, yielding the following expression:

$$\tau_{th} \propto I_p^{1.0} P_{heat}^{-0.56} \delta^{0.2} n_e(0)^{0.3} n_{e,SOL}^{-0.17} \tag{4}$$

with RMSE as low as 9%. This expression reflects the good confinement for peaked density profiles and indicates the moderate confinement degradation with gas puffing represented by $n_{e,SOL}$. The quite low RMSE is not due to the addition of one regressor but is indeed provided by that fact that this variable set may account for the physical situation, as shown by unsuccessful attempts made with other variables.

7. Type-II ELMs: good confinement and low divertor power load

Small high frequency (or grassy) ELMs of type-II were observed in DIII-D [18] and JT-60U [19] whereas the "Enhanced D_α" regime was reported in Alcator-C Mod [20]. These regimes were obtained for $q_{95} \geq 4.5$ and $\delta \geq 0.4$ and at medium density. In ASDEX Upgrade type-II ELMs were identified in a comparable operation region, but just below the Greenwald limit, $\bar{n}_e > 0.8 \times n_{GW}$, [21]. This latter requirement, which differs from what was observed in the

other devices, is quite attractive for a future reactor. In addition the confinement in type-II ELM regimes is almost as good as with type-I ELMs, providing $\tau_{th}/\tau_{IPB98(y)} \approx 0.95$ (see Fig 11), significantly higher than for type-III ELMs. The thermography data of the divertor target plates show that the peak power load is strongly reduced with type-II ELMs, reaching at most 2 MW m^{-2} on the outer plate, in comparison to 5 MW m^{-2} for type-I ELMs. The heat flux with type-II ELMs is quite regular, almost without peaks. The power flux on the inner plates is always very low under these conditions. Magnetic measurements indicate that type-II ELMs often have a precursor at 15 to 30 kHz, indicating that they are MHD events indeed. Their signatures are different from those of type-III ELMs and they provide better confinement because they preserve the high edge pressure, for more detail see [21]. It is not clear yet whether they are in the second stability regime.

Summary and conclusion

Our studies in ASDEX Upgrade show that temperature profiles are stiff in most of the discharges. This implies that global confinement is strongly related to pedestal pressure. Density profiles are not stiff, providing some confinement improvement when it peaks. ECH experiments strongly support the hypothesis that ETG physics with streamers plays a role in electron transport. High density could be reach with type-II ELMs providing a promising regime for a future fusion devices with good confinement and low power load in the divertor. An extended and more detailed version of this paper was submitted to Nuclear Fusion.

Fruitful discussions with F. Jenko and X. Garbet are warmly acknowledged. We are glad to thank the authors of the transport models for having provided their numerical routines.

References

[1] SUTTROP, W. et al., Plasma Phys. Controlled Fusion **39** (1997) 2051.

[2] STOBER, J. et al., Plasma Phys. Controlled Fusion **42** (2000) A211.

[3] KOTSCHENREUTHER, M. et al., Phys. Plasmas **2** (1995) 2381.

[4] PETTY, C. et al., Phys. Rev. Lett. **83** (1999) 3661.

[5] DIMITS, A. et al., Phys. Plasmas **7** (2000) 969.

[6] TARDINI, G. et al., Contr. Fus. Plas. Phys. , 27^{th} EPS Conf., Budapest, Paper P3 82 (2000).

[7] JENKO, F. et al., Phys. Plasmas **7** (2000) 1904.

[8] JENKO, F., Submit. Phys. Rev. Letters (2000) .

[9] WALTZ, R. E. et al., Phys. Plasmas **4** (1997) 2482.

[10] NORDMAN, H. et al., Nucl. Fusion **30** (1990) 983.

[11] PEETERS, A. G. et al., This Conf. Paper EXP5/06 .

[12] JANESCHITZ, G. et al., Contr. Fus. Plas. Phys, 26^{th} EPS Conf. , Maastricht, **23J** (1999) 1445.

[13] RYTER, F. et al., Submit. Phys. Rev. Letters .

[14] LOPES CARDOZO, N. J., Plasma Phys. Contr. Fusion **37** (1995) 799.

[15] JACCHIA, A. et al., Phys. Fluids **B 3** (1991) 3033.

[16] HARTFUSS, H. J. et al., Plasma Phys. Controlled Fusion **36** (1994) B17.

[17] ITER Physics Basis, Chap. II, page 2208, Table 5, Nucl. Fusion **39** (1999).

[18] OZEKI, T. et al., Nucl. Fusion **30** (1990) 1425.

[19] KAMADA, Y. et al., Plasma Phys. Controlled Fusion **42** (2000) A247.

[20] GREENWALD, M. et al., Plasma Phys. Controlled Fusion **42** (2000) A263.

[21] STOBER, J. et al., Submit. Nucl. Fus.